USING FOURIER VELOCITY ENCODED MRI DATA TO GUIDE CFD SIMULATIONS

V. C. Rispoli[⋆] *J.-F. Nielsen*[†] *K. S. Nayak*[‡] *J. L. A. Carvalho*[◇]

[⋆] Engineering Faculty at Gama, University of Brasilia, Brazil. *e-mail: vrispoli@pgea.unb.br*

[†] Biomedical Engineering, University of Michigan, USA. *e-mail: jfnielse@umich.edu*

[‡] Electrical Engineering, University of Southern California, USA. *e-mail: knayak@usc.edu*

[◇] Department of Electrical Engineering, University of Brasilia, Brazil. *e-mail: joaoluiz@pgea.unb.br*

ABSTRACT

Fourier velocity encoding (FVE) is a promising magnetic resonance imaging (MRI) method for assessment of cardiovascular blood flow. FVE provides considerably higher signal-to-noise ratio than phase contrast (PC) imaging, is robust to partial-volume effects and can be acquired rapidly using spiral readouts. On the other hand, FVE data do not directly provide a velocity map. These maps are useful for calculating the actual blood flow through a vessel, or for guiding computational fluid dynamics simulations (CFD). In this paper, FVE data were simulated from PC velocity maps from a pulsatile carotid flow phantom; velocity maps were then reconstructed from these FVE data, and used to guide CFD simulations. FVE-guided CFD velocity fields were qualitatively and quantitatively compared with the PC-measured velocity field, with the pure CFD solution, and with PC-guided CFD. The results show that FVE-guided CFD achieves better agreement with the PC-measured velocity field than pure CFD. Compared with PC-guided CFD, FVE provides considerably better results than PC with similar scan time, and equivalent results when compared with PC with 9 times longer scan time.

***Index Terms*—** Computational fluid dynamics, magnetic resonance imaging, Fourier velocity encoding

1. INTRODUCTION

The current gold standard for magnetic resonance imaging (MRI) flow quantification is phase contrast (PC) [1]. However, PC suffers from partial-volume effects when a wide distribution of velocities is contained within a voxel [2]. Particularly, this is problematic when flow is turbulent and/or complex, or at the interface between blood and vessel wall. This issue is typically addressed by increasing the spatial resolution, which dramatically affects the signal-to-noise ratio (SNR) and increases the scan time.

Fourier velocity encoding (FVE) [3] is an alternative to phase contrast imaging. FVE provides considerably higher SNR than PC, due to its higher dimensionality and larger voxel sizes. Furthermore, FVE is robust to partial voluming, as it resolves the velocity distribution within each voxel. Spiral FVE (sFVE) is a rapid method for FVE-based velocity-distribution measurement [4]. It consists in combining slice-selective spiral imaging along the spatial k-space (k_x-k_y) with phase-encoding along the through-plane velocity (w) Fourier dimension (k_w).

FVE data is usually acquired with low spatial resolution, due to scan-time restrictions associated with its higher dimensionality. FVE is capable of providing the velocity distribution associated with a large voxel, but does not directly provides a velocity map. Velocity maps, however, are useful for calculating the actual blood flow through a vessel, or for guiding computational fluid dynamics simulations [5].

In this paper, sFVE data was simulated from the through-plane velocity component of a 3DFT PC dataset acquired from a pulsatile flow phantom. Then, a velocity map was extracted from the simulated sFVE data, using the methodology proposed in Ref. [6]. Finally, CFD simulations guided by the recovered velocity map were performed using the methodology described in Ref. [5].

2. METHODS

2.1. Data acquisition

High-spatial-resolution four-dimensional PC data of a pulsatile carotid flow phantom (Phantoms by Design, Inc., Bothell, WA) (Fig. 1) were obtained using a 3DFT SPGR pulse sequence. The scan parameters were: $0.5 \times 0.5 \times 1$ mm^3 spatial resolution; field-of-view $4.0 \times 3.5 \times 5.0$ cm^3; TR 11.4 ms; flip angle 8.5°; temporal resolution 91.2 ms; VENC 50 cm/s; 40 min per scan; 9 NEX. The data were acquired on a GE Discovery MR750 3T system, with a 32-channel receive-only head coil array (Nova Medical, Inc., Wilmington, MA, USA). The phantom's pulse cycle was set to 60 bpm. The velocity map for each spatial axis — u_{pc}, v_{pc}, and w_{pc} — was reconstructed using data from all channels of the receive coil array. The lumen was segmented by manually outlining the vessel borders from a stack of 2D axial images, obtained from the reconstructed 3D volume.

978-1-4799-2374-8/15/$31.00 ©2015 IEEE

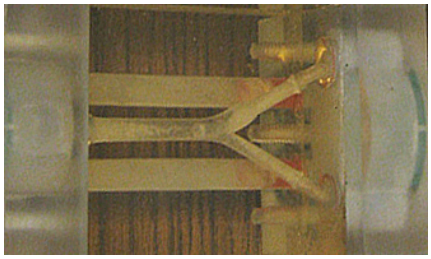

Fig. 1. Pulsatile carotid flow phantom (Phantoms by Design, Inc., Bothell, WA) used to validate the proposed method.

2.2. sFVE Signal Model

If two-dimensional PC is used to measure the through-plane velocities across a vessel, for example, then two two-dimensional functions are obtained: $m(x,y)$ and $w_{\rm pc}(x,y)$, the magnitude and velocity maps, respectively. If these maps are measured with sufficiently high spatial resolution and flow is laminar, one can assume that the spatial-velocity distribution associated with the object is approximately:

$$s(x,y,w) = m(x,y) \times \delta\left[w - w_{\rm pc}(x,y)\right], \qquad (1)$$

where $\delta(\alpha)$ is the Dirac delta function.

The spatial-velocity distribution may be measured in MRI using FVE [3]. Spiral FVE acquisitions follows a stack-of-spirals pattern in k_x-k_y-k_w space (the k-space associated with the $s(x,y,w)$ distribution) [6]; k-space data are truncated to a cylinder with diameter $1/\delta r$ and height $1/\delta w$, where δr and δw are the spatial and velocity resolutions, respectively.

The associated spatial-velocity blurring kernel can be modeled as a convolution of the true distribution $s(x,y,w)$, with $\mathrm{jinc}\left(\sqrt{x^2+y^2}/\delta r\right)$ and $\mathrm{sinc}\left(w/\delta w\right)$, resulting in:

$$\begin{aligned}\hat{s}(x,y,w) &= \left[m(x,y) \times \mathrm{sinc}\left(\frac{w - w_{\rm pc}(x,y)}{\delta w}\right)\right] \\ &* \ \mathrm{jinc}\left(\frac{\sqrt{x^2+y^2}}{\delta r}\right), \end{aligned} \qquad (2)$$

where $\hat{s}(x,y,w)$ is the measured spatial-velocity distribution, $*$ denotes the convolution operation, $\mathrm{sinc}(\alpha) = \sin(\pi\alpha)/(\pi\alpha)$, and $\mathrm{jinc}(\alpha) = J_1(\pi\alpha)/(2\alpha)$, where $J_1(\alpha)$ is a Bessel function of the first kind [7].

Simulated sFVE distributions were derived from the PC data, using the formulation presented in Eq. 2. This was performed only for the through-axis velocity component (w), and for a cardiac phase corresponding to the phantom's mid-systole. The 9-NEX PC dataset was used in this process, so that the FVE distributions were computed from low-noise velocity maps (as in Ref. [4]). This is because FVE has considerably higher SNR than PC in general, due to its higher dimensionality and larger voxel size. Two different sFVE distributions were obtained for each slice of the volume: one using δr = 1 mm, and one using δr = 2 mm. The velocity resolution was $\delta w = 10$ cm/s, over a 120 cm/s velocity field-of-view.

2.3. Estimating the velocity map from a FVE distribution

The deconvolution algorithm proposed in Ref. [8] was then used to reduce spatial blurring effects due to finite spatial resolution in $\hat{s}(x,y,w)$, assuming the blurring kernel to be $\mathrm{jinc}(r/\delta r)$. This deblurred distribution is assumed to be

$$\tilde{s}(x,y,w) \approx m(x,y) \times \mathrm{sinc}\left(\frac{w - w_{\rm pc}(x,y)}{\delta w}\right). \qquad (3)$$

Assuming a high-resolution spin-density map, $\tilde{m}(x,y) \approx m(x,y)$, was available (this could be acquired in a separate scan), the velocity $\hat{w}_{\rm fve}$ associated with a given spatial coordinate (x_o, y_o) could be estimated from $\tilde{s}(x,y,w)$ as:

$$\hat{w}_{\rm fve}(x_o,y_o) = \arg\min_{\omega} \left\| \frac{\tilde{s}(x_o,y_o,w)}{\tilde{m}(x_o,y_o)} - \mathrm{sinc}\left(\frac{w-\omega}{\delta w}\right)\right\|_2, \qquad (4)$$

for $\tilde{m}(x_o,y_o) \neq 0$, otherwise $\hat{w}_{\rm fve}(x_o,y_o) = 0$.

This minimization process was used to reconstruct estimated velocity maps from the simulated sFVE distributions. The spin-density map from the PC acquisition was used as our high-resolution map, $\tilde{m}(x,y)$. This was repeated for each pixel of each slice of the volume, and for both values of δr.

2.4. FVE-guided computational fluid dynamics

Computational fluid dynamics calculations guided by MRI data were performed using a modified version of the SIMPLER algorithm [5]. The phantom's blood mimicking fluid was assumed to be a Newtonian, isothermal, and incompressible fluid, with constant viscosity μ and density ρ.

The discretization of the Navier–Stokes equations [9], given by:

$$\rho\left(\frac{\partial \vec{\nu}}{\partial t} + \vec{\nu}\cdot\nabla\vec{\nu}\right) = -\nabla p + \mu\Delta\vec{\nu}, \qquad (5)$$

where $\vec{\nu} = (u,v,w)$ is the velocity field, produces three linear systems:

$$\mathbf{A}_{u,n}\boldsymbol{u}_{n+1} = \mathbf{b}_{u,n}, \qquad (6)$$

$$\mathbf{A}_{v,n}\boldsymbol{v}_{n+1} = \mathbf{b}_{v,n}, \quad \text{and} \qquad (7)$$

$$\mathbf{A}_{w,n}\boldsymbol{w}_{n+1} = \mathbf{b}_{w,n}, \qquad (8)$$

where $\mathbf{A}_{u,n}$, $\mathbf{A}_{v,n}$, and $\mathbf{A}_{w,n}$ are hepta-diagonal square matrices containing information about μ, ρ and the velocities from the previous time iteration; and $\mathbf{b}_{u,n}$, $\mathbf{b}_{v,n}$, and $\mathbf{b}_{w,n}$ are column vectors also containing information about μ, ρ, previous iteration velocities and pressure.

In the proposed approach, additional rows are included in matrices $\mathbf{A}_u$, $\mathbf{A}_v$, and $\mathbf{A}_w$, and in vectors $\boldsymbol{b}_u$, $\boldsymbol{b}_v$, and $\boldsymbol{b}_w$, in order to incorporate the MRI-measured velocity values. This

approach assumes that the velocity measured with PC-MRI for a given voxel can be expressed as a linear combination of the velocities on the underlying CFD calculation grid. The new overdetermined systems are solved in the least-squares sense for each step of the SIMPLER algorithm. The algorithm calculations are performed forward in time in order to obtain a steady-state solution, i.e.:

$$\vec{\nu}_\infty = \lim_{t\to\infty} \vec{\nu}(t). \quad (9)$$

Each of the two $\hat{w}_{\rm fve}(x, y, z)$ velocity maps reconstructed from the simulated sFVE distributions — one for δr = 1 mm, and one for δr = 2 mm — were used to guide a CFD solution. Calculations assumed fluid viscosity of $\mu = 0.005$ Pa·sec and density of $\rho = 1100$ kg/m^3 (values provided by manufacturer), and were performed with time step $\delta t = 0.25$ ms on a Cartesian grid of $0.5\times0.5\times1$ mm^3 voxel size. The CFD simulation domain was rectangular of size $32.5\times9.0\times41.0$ mm^3. Each iteration required about 10 seconds of computation time on an Intel Core i7 processor running at 2.8 GHz.

The two FVE-guided CFD velocity fields were qualitatively and quantitatively compared with the PC-measured velocity field; with the pure CFD solution, i.e., a CFD solution which uses MRI measurements — $\vec{\nu}_{\rm pc} = (u_{\rm pc}, v_{\rm pc}, w_{\rm pc})$ — only as inlet and outlet boundary conditions; and with two PC-guided CFD velocity fields: one obtained using a single NEX of the PC scan (which corresponds to approximately the same scan time as the FVE scan with δr = 1 mm), and one obtained using all 9 NEX (i.e., 9 times longer scan time).

2.5. Quantitative evaluation

The CFD-simulated velocity fields were quantitatively compared with the PC measurements by means of the signal-to-error ratio (SER). We considered the PC velocity field, $\vec{\nu}_{\rm pc}$, as our ground-truth "signal"; consequently, the estimation error is the vector difference between the CFD-estimated velocity field, $\vec{\nu}_\infty = (u_\infty, v_\infty, w_\infty)$, and the ground-truth field, $\vec{\nu}_{\rm pc}$. Thus, the SER is calculated (in decibels) as:

$$\mathrm{SER}_{\vec{\nu}} = 10\log_{10}\left(\frac{\sum_{i,j,k}\|\vec{\nu}_{\rm pc}(i,j,k)\|^2}{\sum_{i,j,k}\|\vec{\nu}_\infty(i,j,k)-\vec{\nu}_{\rm pc}(i,j,k)\|^2}\right), \quad (10)$$

where integers i, j, and k represent grid-point indexes along the x, y, and z axes, respectively. The SER was also calculated individually for u, v, and w. Using these SER values, the CFD approaches — pure CFD, and CFD driven by $\hat{w}_{\rm fve}$ — were quantitatively evaluated and compared.

3. RESULTS

The spin-density maps shown in Fig. 2a illustrate the spatial blurring associated with each value of δr, for a slice perpendicular to the phantom's bifurcation. Fig. 2b presents the FVE-estimated velocity maps, $\hat{w}_{\rm fve}$, for each spatial resolution value. Fig. 2c shows the associated errors (relative to the PC map, $w_{\rm pc}$, shown in Fig. 2b, left). The results show that lower error levels were obtained when FVE data with finer spatial resolution was used. In this slice, the absolute error was greater than 5 cm/s for only 9% of the voxels when $\delta r = 1$ mm was used; while 26.5% of the voxels presented error greater than 5 cm /s when $\delta r = 2$ mm was used.

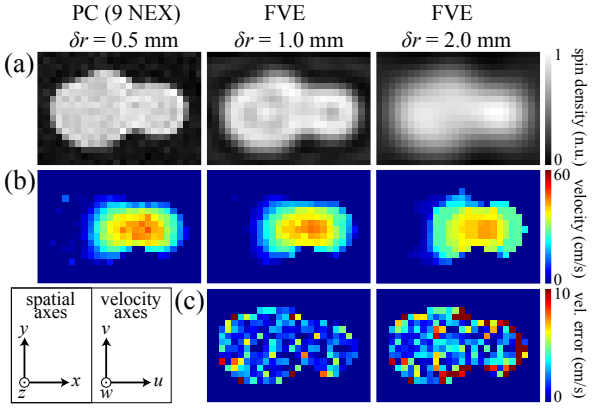

Fig. 2. (a) Spin-density maps for PC (0.5 mm spatial resolution, 9 NEX), FVE with 1 mm spatial resolution, and FVE with 2 mm spatial resolution, for a slice perpendicular to a carotid phantom's bifurcation; (b) corresponding velocity maps; and (c) absolute error for the FVE-estimated velocity maps, relative to the PC reference.

Figure 3 shows the PC-measured velocity field; and the CFD-simulated velocity fields, obtained using pure CFD, PC-driven CFD (1 and 9 NEX), and FVE-driven CFD (δr = 1 and 2 mm). Considerable qualitative improvement – with respect to agreement with the PC reference – can be appreciated in the FVE-driven results, when compared with the pure CFD result and with PC-driven CFD with similar scan time (1 NEX).

Finally, Table 1 presents the measured SER relative to the PC reference, for the CFD results shown in Fig. 3. Both FVE-driven solutions achieved higher SER than pure CFD and single-NEX PC-driven CFD. When evaluating the three-dimensional velocity vector $\vec{\nu}$, the SER gain relative to pure CFD was 1.49 dB for $\delta r = 1$ mm, and 0.80 dB for $\delta r = 2$ mm; relative to single-NEX PC-driven CFD the gain was 3.65 dB for $\delta r = 1$ mm (similar scan time), and 2.96 dB for $\delta r = 2$ mm (3 times faster); relative 9-NEX PC-driven CFD (which requires much longer scan time), the SER was only 0.32 dB lower for $\delta r = 1$ mm (9 times faster), and only 1.01 dB lower for $\delta r = 2$ mm (27 times faster). When evaluating only the y-axis velocity component (v), there was a 0.11-0.35 dB loss in SER (relative to pure CFD) with the proposed method. This is most likely be a positive effect of denoising, since the velocities along that axis are extremely low ($v_{\rm pc}$'s total energy is 15.7 dB lower than that of $w_{\rm pc}$). Nevertheless, the SER gains for the u and w components more than compensate for this.

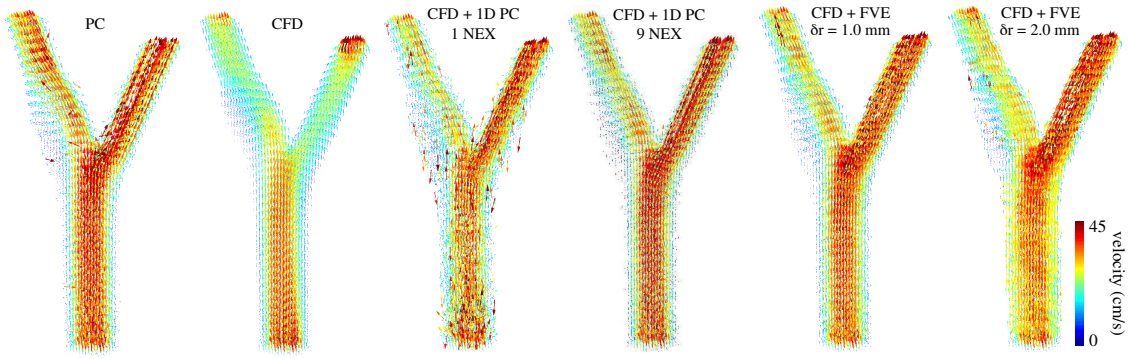

Fig. 3. Vector field visualization of the velocity field ($\vec{v}$) over the entire tridimensional volume of the carotid bifurcation of the phantom: PC; pure CFD; CFD guided by w_{pc}, reconstructed from 1 NEX and 9 NEX; CFD guided by $\hat{w}_{\mathrm{fve}}$, recovered from simulated sFVE data with $\delta r = 1.0$ mm and 2.0 mm.

Table 1. Signal-to-error ratio between each of the CFD approaches and the PC reference.

	pure CFD	**CFD + 1D PC** 1 NEX	**CFD + 1D PC** 9 NEX	**CFD + sFVE** $\delta r = 1.0$ mm	**CFD + sFVE** $\delta r = 2.0$ mm
SER_u	2.97 dB	2.72 dB (↓)	4.16 dB (↑)	3.93 dB (↑)	3.81 dB (↑)
SER_v	−0.25 dB	−0.88 dB (↓)	−0.30 dB (↓)	−0.36 dB (↓)	−0.60 dB (↓)
SER_w	5.44 dB	6.21 dB (↑)	16.53 dB (↑↑↑)	10.97 dB (↑↑)	7.22 dB (↑)
$\mathrm{SER}_{\vec{v}}$	6.57 dB	4.41 dB (↓)	8.38 dB (↑)	8.06 dB (↑)	7.37 dB (↑)

4. CONCLUSIONS

This work presented a method for using FVE data to guide CFD simulations. The results show that FVE-guided CFD achieves better agreement with the PC-measured velocity field than pure CFD. Compared with PC-guided CFD, FVE provides considerably better results than PC with similar scan time. This is because a 1-mm resolution sFVE dataset could be acquired in the same scan time as 1 NEX of a 0.5-mm resolution PC dataset with the above parameters; however the FVE dataset would have SNR 23 dB higher than that of PC (the scan time of 2-mm resolution sFVE would be 3 times shorter, and the SNR would still be 8 dB higher than that of PC). When compared with CFD guided by high-SNR PC, FVE provides equivalent results in much shorter scan time.

5. REFERENCES

[1] M. O'Donnell, "NMR blood flow imaging using multi-echo, phase contrast sequences," *Med. Phys.*, vol. 12(1), pp. 59–64, 1985.

[2] C. Tang, D. D. Blatter, and D. L. Parker, "Accuracy of phase–contrast flow measurements in the presence of partial–volume effects," *J. Magn. Reson. Imaging*, vol. 3(2), pp. 377–385, 1993.

[3] P. R. Moran, "A flow velocity zeugmatographic interlace for NMR imaging in humans," *Magn. Reson. Imag.*, vol. 1, pp. 197–203, 1982.

[4] J. L. A. Carvalho, J. F. Nielsen, and K. S. Nayak, "Feasibility of *In Vivo* measurement of carotid wall shear rate using spiral Fourier velocity encoded MRI," *Magn. Reson. Med.*, vol. 63, pp. 1537–1547, 2010.

[5] V. C. Rispoli, J.-F. Nielsen, K. S. Nayak, and J. L. A. Carvalho, "Computational fluid dynamics simulations guided by 3D PC-MRI data," in *Proc. Intl. Soc. Mag. Reson. Med. 22*, Milan, IT, 2014, p. 2490, ISMRM.

[6] V. C. Rispoli and J.L.A. Carvalho, "Deriving high–resolution velocity maps from low-resolution Fourier velocity encoded MRI data," in *IEEE 10th ISBI*, San Francisco, CA, USA, 2013, pp. 334–337, IEEE.

[7] D. Nishimura, *Principles of Magnetic Resonance Imaging*, Stanford University Press, Stanford, CA, USA, 1st edition, 2010.

[8] D. Krishnan and R. Fergus, "Fast image deconvolution using hyper–Laplacian priors," in *NIPS 22*, Vancouver, CA, 2009, pp. 1033–1041, Curran Associates, Inc.

[9] H. Versteeg and W. Malalasekera, *An Introduction to Computational Fluid Dynamics: The Finite Volume Method*, Prentice-Hall, Glasgow, SCT, UK, 2nd edition, 2007.